Journal of Statistical Physics, Vol. 121, Nos. 1/2, October 2005 (© 2005)
DOI: 10.1007/s10955-005-7001-6

Dynamics of Interface Displacement in Capillary Flow

Luís O. E. dos Santos[1], Fabiano G. Wolf[1], and Paulo C. Philippi[1]

Received October 12, 2004; accepted May 20, 2005

The dynamics of capillary flow has several practical applications in the industry and has been extensively investigated. The main focuses in these studies are the motion of the interface, especially near the three-phase contact line, and the change of contact angle during the invasion process. In this work we present several simulations results of capillary invasion in two- and three-dimensions, using the Lattice–Boltzmann model based on field mediators. We investigate the velocity field near the solid surface, the changes in the contact angle as a consequence of the flow, and the boundary conditions that can be used in the inlet and outlet of the capillary tube. In all simulations the diameter of tube is made large enough to enable the evaluation of the contact angle directly from the density field and the results of capillary rise are compared with a theoretical model based on the Bosanquet equation, which includes capillary, viscous, inertial and gravitational effects.

KEY WORDS: Lattice–Boltzmann method (LBM); immiscible fluids; capillary flow.

1. INTRODUCTION

Capillary invasion in small cavities is an important immiscible displacement problem in several research areas, with growing economical and scientific interest. In spite of several achievements,[1–7] the complete understanding of the problem remains to be achieved. The problem basically consists in the immersion of a capillary tube inside a fluid at rest and involves three phases: a wetting fluid, a non-wetting fluid, and a solid surface. Depending on the wetting conditions, summarized by the contact angle, the wetting fluid can invade the capillary, reaching an equilibrium height h_{eq}, or can be repelled, creating a depression in the region

[1]Mechanical Engineering Department, Federal University of Santa Catarina, 88040-900, Florianópolis, SC, Brazil; e-mails: {fgwolf,philippi}@lmpt.ufsc.br

immersed. Due to its potentiality for simulating immiscible fluids, the Lattice–Boltzmann method seems to be a valuable tool for studying this phenomenon. In the following sections, after a brief review of capillary flow (Section 2), a lattice–Boltzmann immiscible fluids model based on field mediators is presented (Section 3). In Section 4, simulation results and comparisons with theoretical predictions are presented. Section 4 has three subsections, focusing the boundary conditions used, the 2D and the 3D simulations, respectively.

2. CAPILLARY INVASION

Lucas,[8] in 1918, and Washburn,[1] in 1921, were the first who described the dynamics of capillary rise. They considered the invasion as being determined by a balance among capillary, gravitational and viscous forces. Poiseuille profile was taken as the velocity profile. The Lucas–Washburn equation has been confirmed by experimental data,[7] and is considered as a valid approximation, although it fails to describe the initial stages of the invasion since it does not consider the inertial effects, important in the early beginning of the process.[5] Inertial effects were considered by Bosanquet, who proposed an alternative approach to the Lucas–Washburn model, in 1923. Another model was proposed by Szekely *et al.*,[2] including the outside flow effects (entrance effects). Since the main intention in this paper is to compare the Lattice–Boltzmann method with a theoretical model and not with experimental results, entrance effects were not considered in the present formulation. Therefore, in this work, LB results are compared with the Bosanquet model, which was rewritten considering both fluids with the same density ($\rho_R = \rho_B = \rho$) and the same viscosity ($\mu_R = \mu_B = \mu$), giving,

$$\frac{d^2h(t)}{dt^2} + \frac{(D^2-1)\mu}{r^2\rho}\frac{dh(t)}{dt} = \frac{(D-1)\sigma\cos\theta}{r\rho H} - \frac{gh(t)}{H}, \tag{1}$$

where D is the space dimension, $D = 2$ for parallel plates, and $D = 3$ for cylindrical capillaries and r is the capillary radius, Fig. 1. The other parameters in Eq. (1), σ, θ, g and H are, respectively, interfacial tension, contact angle, gravitational acceleration, and capillary length.

3. IMMISCIBLE LATTICE–BOLTZMANN

In this work, a lattice–Boltzmann model based on field mediators was employed. The model is fully described in ref. 9 and some slight improvements commented at the end of this section, were performed. Two particle

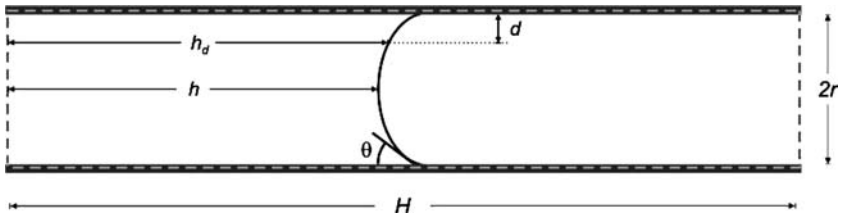

Fig. 1. Measure of the contact angle θ.

distribution functions, R_i and B_i, are used to describe the immiscible fluids r and b. Particles interaction is modeled by splitting the BGK collision term, considering, separately, $r-r$ and $r-b$ collisions. A third distribution function – namely, the mediator's distribution function M_i – is used to model the long range interaction, carrying out neighborhood information. The distribution functions are updated considering two steps:

(a) *local step* – involving the particles collision process and the emission/ annihilation of the field mediators;

(b) *non-local step*, i.e., the propagation step.

In what follows, $\mathbf{X}$ is the position vector and $\mathbf{c}_i$ is a discrete velocity. In the local step particle distributions are updated at each time step T by a collision process:

$$R_i' = R_i + \omega^r \frac{R_i^0(\rho^r, \mathbf{u}^r) - R_i}{\tau^{rr}} + \omega^b \frac{R_i^0(\rho^r, \vec{\vartheta}^b) - R_i}{\tau^m}, \tag{2}$$

$$B_i' = B_i + \omega^b \frac{B_i^0(\rho^b, \mathbf{u}^b) - B_i}{\tau^{bb}} + \omega^r \frac{B_i^0(\rho^b, \vec{\vartheta}^r) - B_i}{\tau^m}, \tag{3}$$

where

$$\rho^k = \sum_{i=0}^{b_m} K_i\,, \qquad \mathbf{u}^k = \frac{1}{\rho^k} \sum_{i=1}^{b_m} K_i \mathbf{c}_i\,, \tag{4}$$

are, respectively, the macroscopic density and the velocity of component k, $k = r, b$. R_i^0 and B_i^0 are the equilibrium distributions. The ω's are the mass fractions, $\omega^k = \rho^k/\rho$. The ϑ's are the local velocities modified by the action of mediators,

$$\vec{\vartheta}^r = \mathbf{u}^r + A\widehat{\mathbf{u}}^m, \qquad \vec{\vartheta}^b = \mathbf{u}^b - A\widehat{\mathbf{u}}^m \tag{5}$$

and

$$\hat{\mathbf{u}}^m = \frac{\sum_i M_i \mathbf{c}_i}{\left|\sum_i M_i \mathbf{c}_i\right|}. \tag{6}$$

The mediator's distribution are updated by an *emission/annihilation* step, defined by

$$M_i' = \alpha M_i + \beta \frac{R_i}{R_i + B_i}, \tag{7}$$

where α and β are weights used for settling the interaction length.[9] The propagation step is the only non-local step and is identical for all the distributions,

$$K_i(\mathbf{X} + \mathbf{c}_i, T + 1) = K_i'(\mathbf{X}, T), \tag{8}$$

where $K = R, B$ or M. The model described in this section differs from the model previously proposed in Santos *et al.*[9] in two points:

(a) A single distribution function is used for describing the distribution of mediators, instead of two, as in the previous model. This modification can be considered as a computational improvement and does not change the theoretical aspects of the model, since, in the previous model, the mediators–particles interaction rules were, effectively, based on the difference between the two distributions.

(b) The emission/annihilation step (see Eq. (7)) was previously written $M_i^{r\prime} = \alpha M_i^r + \beta w^r$. In our simulations, this change appears to decrease the magnitude of the spurious currents, although a more detailed analysis remains to be done.

4. COMPARISON BETWEEN THEORETICAL PREDICTIONS AND SIMULATION RESULTS

All simulations were performed using the model described above, setting $\tau^{rr} = \tau^{bb} = \tau^m = 1.0$, $A = 0.4$ and $\alpha = 0$, $\beta = 1$, employing a D3Q19 lattice (even in the 2D simulations). Both densities were put equal to unity, $\rho^r = \rho^b = 1$, and the resulting viscosities and interfacial tension were $\nu^r = \nu^b = 1/6$ and $\sigma = 0.333$, respectively. The contact angle θ was obtained

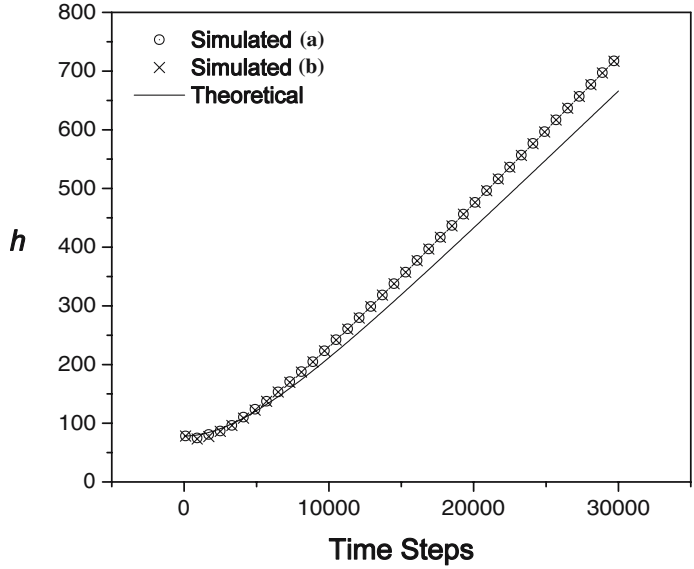

Fig. 2. Boundary conditions (a) and (b), without gravity, $H = 800$.

directly from the density fields by the position of the interface in two points, h and h_d (see Fig. 1), applying the expression:

$$\cos\theta = \frac{2r\,(h_d - h)}{(h_d - h)^2 + (r - d)^2}. \tag{9}$$

A simple analytical solution of Eq. (1) can be obtained when $g = 0$,

$$h(t) = \frac{(D-1)\sigma r\cos\theta}{(D^2-1)^2\mu^2 H}\left\{r^2\rho\exp\left[-\frac{(D^2-1)\mu t}{r^2\rho}\right] + (D^2-1)\mu t - r^2\rho\right\}. \tag{10}$$

The solution above was used in comparison with simulations (Figs. 2 and 8).

4.1. Boundary Conditions

At the solid surface, bounce back boundary conditions for the particle distributions were imposed. The boundary conditions for the mediators distribution try to modulate the interaction process between the solid and

the fluid. The wettability, or the desired contact angle, can be obtained by imposing, at each fluid site adjacent to a solid site, a constant value M_i^{solid} for the mediator distribution along the directions i leading to the fluid phase in the propagation step. This quantity determines the contact angle, since it determines the interaction between solid and fluids. As the mediator distribution carries the values of mass fraction, $M_i \in [0, 1]$, when $M_i^{\text{solid}} = 1/2$ the contact angle will be $\theta = 90°$. When $M_i^{\text{solid}} > 1/2$, fluid r will behave as the wetting fluid, and when $M_i^{\text{solid}} < 1/2$, fluid b will behave as the wetting fluid. Nevertheless, the precise value of the contact angle also depends on the relaxation parameters (τ_{rr}, τ_{bb}, τ_m). Aiming to compare the simulations with the theoretical model presented in Section 1, which do not consider entrance effects or the influence of the flow outside the capillary, inlet and outlet boundary conditions were imposed in the edges of the capillary, without a reservoir outside the capillary as presented in ref. 6. Two boundary conditions were applied with similar results: (a) *null derivative condition* in the direction of the flow were obtained by imposing that sites in the entrance, $h = 0$, assume the velocity of the adjacent sites ($h = 1$), and analogous were done in the outlet; (b) *quasi-periodic boundary condition* were applied by imposing that any r fluid exiting in the one edge sites (say, the exit) reenters in the other edge sites (the entrance), relabeled as b fluid. In case (a) the density were kept constant and equal in both edges.

4.2. 2D Simulations

In Fig. 2, a comparison is made among the simulation results for a channel length $H = 800$, using boundary conditions (a) and (b) with the theoretical results given by the solution of Bosanquet equation, Eq. (10). Theoretical results for boundary conditions (a) and (b) match very well, but there is a 6.8% difference between the theoretical and simulated results for the steady state interface velocity. The source of this discrepancy can be attributed to the theoretical model itself, since it admits a parabolic flow pattern along the capillary. The parabolic flow profile is not the true velocity profile in capillary invasion, specially, near the interface. This can be noticed in Fig. 3, where the velocity field in capillary flow is displayed. In fact, the flow near the interface can be much more complicated, as can be seen in Fig. 4a, where the streamlines corresponding to the simulations discussed above are shown. Flow is altered by spurious currents (see ref. 9). For evaluating this influence, the same streamlines are shown, in Fig. 4b, corresponding to an analogous simulation, but with the capillary axis inclined in the lattice diagonal direction. In Fig. 4a, spurious

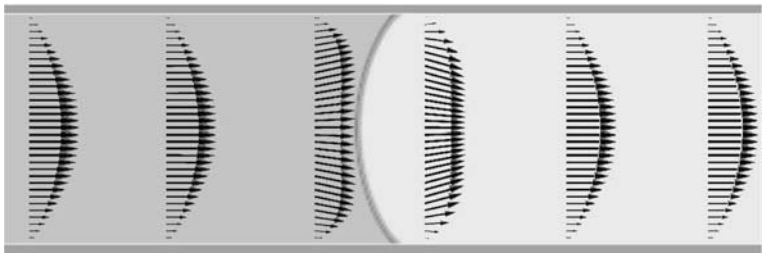

Fig. 3. Velocity field in a capillary invasion.

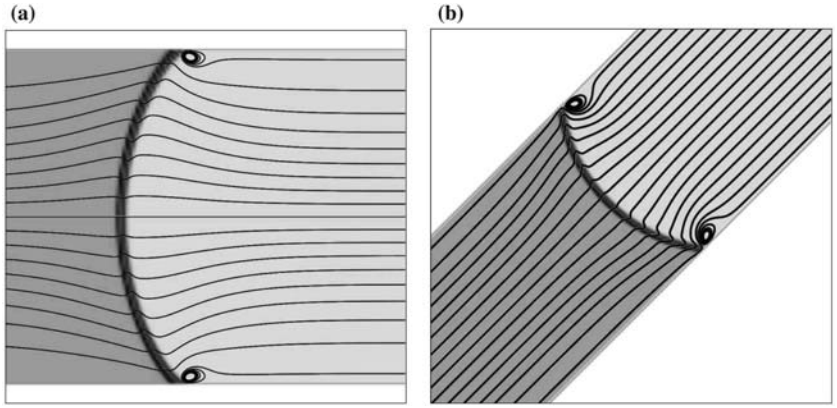

Fig. 4. Stream lines near the interface in capillary invasions: (a) Stream lines corresponding to the simulation presented in Fig. 3; (b) Stream lines corresponding to a simulation in diagonal direction.

currents force the flow along the directions oriented toward the center of the capillary and in Fig. 4b, flow is forced in the opposite directions. Nevertheless, it is important to notice that spurious currents have no influence on the dynamic displacement of the interface, the flow outside the transition layer being unaffected, in both cases. The discrepancy between theoretical and simulated results can be reduced increasing the length of the capillary, since, in this case, the influence of the interfacial flow on the overall process is reduced. In a similar simulation, with $H = 1200$, the disagreement decreases to 5.9% in the invasion velocity, comparing theoretical and simulated results.

In Fig. 5 simulation results are presented and compared with theoretical results, obtained from Eq. (1), considering the influence of gravity, with $g = 10^{-5}$ (in lattice units).

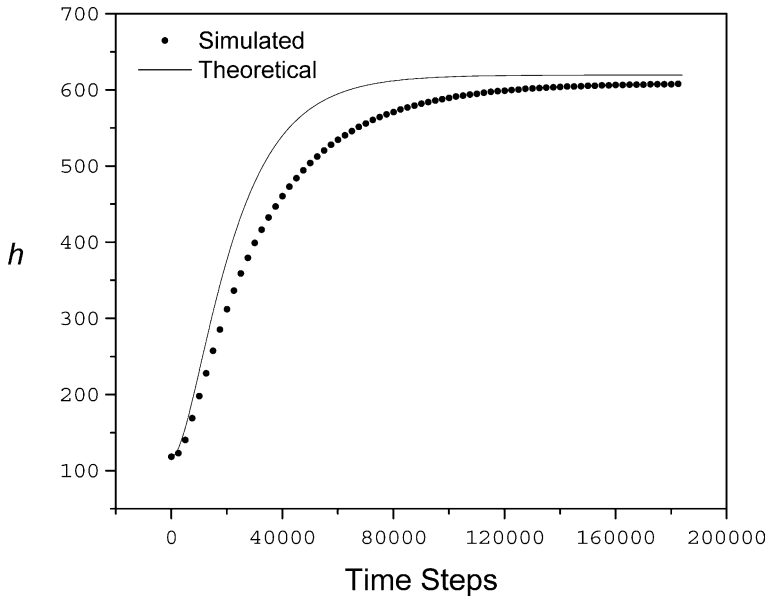

Fig. 5. Capillary invasion using boundary condition(a), $g = 10^{-5}$, $H = 1200$.

Since the theoretical models does not consider the dynamic dependence of the contact angle with the capillary number, there is a discrepancy between theoretical and simulated results (experimental results show similar discrepancies when compared with constant contact angle theoretical models[3]). It is usual, in studies of capillary-rise dynamics, to consider that the contact angle varies according to expression:

$$\cos\theta_d = \cos\theta - \alpha Ca^{\beta}, \tag{11}$$

where θ_d is the dynamic contact angle, α and β are constants, and

$$Ca \equiv \frac{\mu}{\sigma}\frac{dh}{dt} \tag{12}$$

is the capillary number. In Fig. 6 it is shown the dependence of $\cos\theta_d$ on the capillary number obtained from LB simulations. The graph shows that the expression given by Eq. (11) represents adequately the contact angle dependence on Ca. It is seen that Eq. (11) fits very well with simulation results when $\alpha = 18.21$ and $\beta = 0.88$.

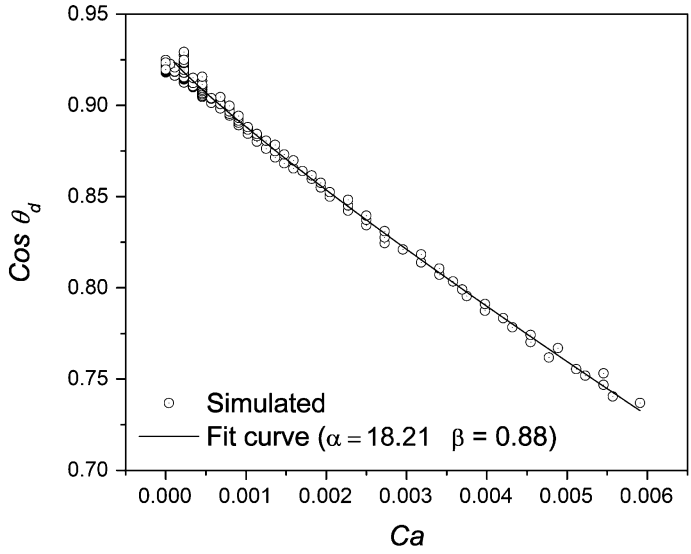

Fig. 6. Dynamic contact angle as a function of the capillary number Ca.

4.3. 3D Simulations

A capillary invasion process in a cylindrical capillary was simulated using the null derivative boundary condition in the inlet and outlet, as explained above. Given the symmetries, only one quarter of the capillary tube was effectively simulated (see Fig. 7), using specular reflection boundary condition at the faces dividing the tube (faces A and B in Fig. 7). The simulated results and the results given by the Bosanquet equation, Eq. (10), are presented in Fig. 8. Although the 4.5% disagreement for the steady state interface velocity is reduced, when compared to the 2D simulation results (6.8%), simulation, now, predicts a smaller interface velocity when compared to the theoretical model. This probably happens due to the discretization effects in the 3D geometrical representation. In fact, in its 3D representation the cylindrical solid surface is rough and has its internal area increased.

5. CONCLUSION

The simulations and comparisons with theoretical predictions presented in this work indicate the potential of the Lattice Boltzmann method in capillary invasion dynamic studies. Two boundary conditions were investigated, showing similar results. The 3D simulations show the

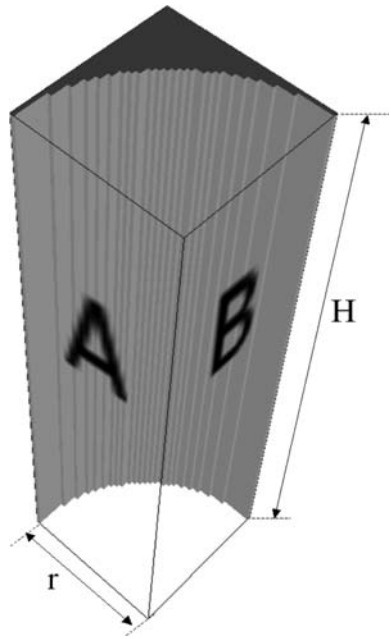

Fig. 7. One quarter of a cylindrical capillary, the faces A and B divide the tube.

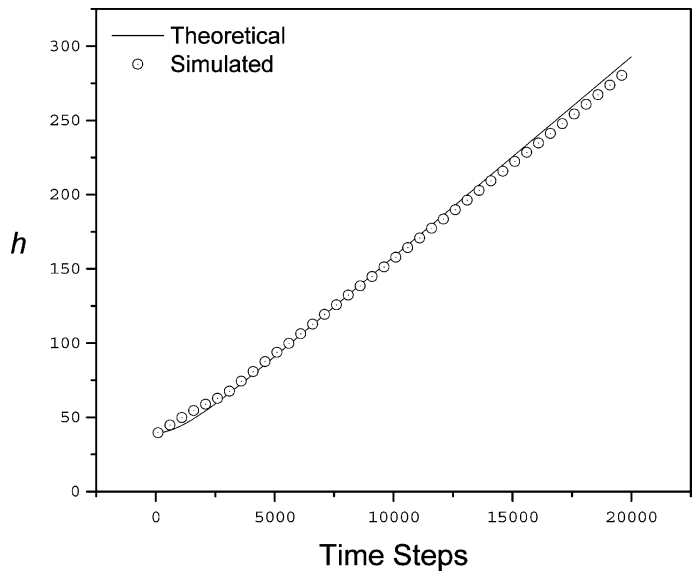

Fig. 8. Invasion of a cylindrical capillary with null derivative boundary condition(a), $g = 0$, $H = 800$, $r = 40$.

possibility of simplifications that can be achieved considering the symmetries of the problem. Comparisons with experimental results remain, yet, to be done.

ACKNOWLEDGMENTS

Authors are greatly indebted to ANP (Brazilian Petroleum Agency), CNPq (Brazilian Research Council), Finep (Brazilian Agency for Research and Projects) and Petrobras (Brazilian Petroleum Company) for the financial support.

REFERENCES

1. E. W. Washburn, The dynamics of capillary flow. *Phys. Rev.* **17**:273–283 (1921).
2. J. Szekely, A. W. Neumann, and Y. K. Chuang, Rate of capillary penetration and applicability of Washburn equation. *J. Colloid. Interf. Sci.* **69**(3):486–492 (1979).
3. T. E. Mumley, C. J. Radke, and M. C. Williams, Kinetics of liquid/liquid capillary rise. 1.Experimental observations. *J. Colloid. Interf. Sci.* **109**(2):398–412 (1986).
4. T. E. Mumley, C. J. Radke, and M. C. Williams, Kinetics of liquid/liquid capillary rise. 2.Development and test of theory. *J. Colloid. Interf. Sci.* **109**(2):413–425 (1986).
5. K. G. Kornev, and A. V. Neimark, Spontaneous penetration of liquids into capillaries and porous membranes revisited. *J. Colloid. Interf. Sci.* **235**(1):101–113 (2001).
6. P. Raiskinmaki, A. Shakib-Manesh, A. Jasberg, A. Koponen, D. Merikoski, and J. Timonen, Lattice-Boltzmann simulation of capillary rise dynamics. *J. Stat. Phys.* **107**(1–2):143–158 (2002).
7. L. R. Fisher, and P. D. Lark, Experimental study of the Washburn equation for liquid flow in very fine capillaries. *J. Colloid. Interf. Sci.* **69**(3):486–492 (1979).
8. R. Lucas, Ueber das Zeitgesetz des Kapillaren Aufstiegs von Flussigkeiten. *Kolloid Z.* **23**:15 (1918).
9. L. O. E. Santos, P. C. Facin, and P. C. Philippi, Lattice-Boltzmann model based on field mediators for immiscible fluids. *Phys. Rev. E* **68**(5):056302 (2003).